Derivation of effective penetration depth of femtosecond laser pulses in metal from ablation rate dependence on laser fluence, incidence angle, and polarization

AUTHOR(S):

Miyasaka, Yasuhiro; Hashida, Masaki; Nishii, Takaya; Inoue, Shunsuke; Sakabe, Shuji

APPLIED PHYSICS LETTERS **106**, 013101 (2015)

Derivation of effective penetration depth of femtosecond laser pulses in metal from ablation rate dependence on laser fluence, incidence angle, and polarization

Yasuhiro Miyasaka, Masaki Hashida, Takaya Nishii, Shunsuke Inoue, and Shuji Sakabe
Advanced Research Center for Beam Science, Institute for Chemical Research, Kyoto University, Gokasho, Uji, Kyoto 611-0011, Japan and Department of Physics, Graduate School of Science, Kyoto University, Kitashirakawa, Sakyo, Kyoto 606-8502, Japan

(Received 26 November 2014; accepted 20 December 2014; published online 5 January 2015)

Ablation rate dependence on laser fluence for copper subjected to oblique femtosecond laser irradiation has been determined experimentally in order to investigate processing induced by oblique irradiation. A difference of ablation rate between *p*-polarized and *s*-polarized oblique irradiation is clearly observed. Effective penetration depth is defined to explain the ablation rate dependence instead of using optical penetration depth, which is treated as a key value for determining the ablation rate in conventional theory. The effective penetration depth for copper is presented in simple formulas as a function of laser incidence angle for each polarization. © *2015 AIP Publishing LLC*. [http://dx.doi.org/10.1063/1.4905353]

Femtosecond lasers are candidates for high value-added processing of metals, particularly when minimal thermal metamorphism,[1,2] self-construction of characteristic surface morphology,[3–6] micromachining,[7] or extremely shallow ablation[8,9] is desired. Ablation rate is a fundamental parameter for controlling laser processing, such as drilling, scraping, and cutting, and for estimating the damage threshold of optical components. Additionally, recent research has demonstrated that the ablation rate is related to the formation of laser-induced surface structures.[10,11] For normal laser incidence, the dependence of ablation rate on laser fluence has been investigated for various metals, pulse widths, wavelengths, and atmospheric pressures.[12–24] Three fluence ranges (high, middle, and low) with distinct ablation rates have been reported for all metals.[12] In the conventional theory derived from a one-dimensional two-temperature model,[25] ablation rates in high and middle fluence ranges are expressed by the following equation:[14]

$$L = l\ln(F/F_{\mathrm{th,h}}), \quad F_{\mathrm{th,h}} = lE_{\mathrm{th}}/(1-R_{\mathrm{h}}), \tag{1}$$

$$L = d\ln(F/F_{\mathrm{th,m}}), \quad F_{\mathrm{th,m}} = dE_{\mathrm{th}}/(1-R_{\mathrm{m}}), \tag{2}$$

respectively. Here, L is the ablation rate, l is the hot electron diffusion length, d is the optical penetration depth, E_{th} is the evaporation threshold energy per volume, F is the laser fluence, $F_{\mathrm{th,h}}$ and $F_{\mathrm{th,m}}$ are the ablation threshold fluences for the high and middle fluence ranges, and R_{h} and R_{m} are the reflectance for high and middle fluences, respectively. The parameters l and d correspond to the slopes of lines in a semi-log plot of ablation rate as a function of fluence, and the reflectance affects only the ablation threshold fluence. In the conventional theory, hot electron diffusion length and optical penetration depth have been treated as key values for determining the ablation rate at high and middle fluences, respectively,[14] therefore, the slopes of the lines do not depend on the reflectance. This logarithmic dependence has been widely used to explain experimental results.[14–17] On the other hand, for oblique irradiation the ablation rate has not been reported. Only ablation efficiency is discussed from the point of view of absorptance dependence on laser incidence angle and polarization.[26–28] Assuming only that the parameters l and d do not depend on laser incidence angle and polarization, a discussion limited to absorptance dependence is valid. However, the measurements reported in this paper reveal that the parameter d behaves differently from the theoretically obtained optical penetration depth. The ablation rate dependence on laser fluence for oblique irradiation would give us fundamental knowledge to help us understand the femtosecond laser-metal interaction and the mechanisms of ablation phenomena depending on laser incidence angle such as laser-induced surface morphology[29–31] and ion emission.[32–34]

In this paper, the dependence of the copper ablation rate on laser fluence is reported for normal incidence and for various incidence angles with *p*- and *s*-polarizations. The obtained ablation rates for oblique incidence show logarithmic dependence as for normal incidence. However, differences in ablation rate dependence on incidence angle and polarization cannot be explained only by the optical absorptance calculated by Fresnel equations. The parameter d corresponding to the optical penetration depth in the middle fluence range depends strongly on the incidence angle and polarization, in contrast to the theoretically calculated optical penetration depth, which depends only minimally on incidence angle. Ablation efficiency in the middle fluence range is discussed not only in terms of absorptance but also effective penetration depth.

The target is mechanically polished bulk copper (99.99% pure), which is attached to a mirror holder mounted on translation stages in air. The arithmetic mean roughness of the target is less than 2 nm. The accuracy of the target surface position is $\pm 5\,\mu$m, which was confirmed by a laser displacement sensor (LK-G15, Keyence). For this study, 10 Hz laser pulses are provided from a chirped pulse amplification T^6 laser system (ICR, Kyoto University). The pulse duration is 45 fs and the center wavelength is 805 nm. The *s*- and

p-polarized laser pulses are focused with a lens ($f = 100$ mm) onto the target at incidence angles θ of 0°, 25°, 45°, and 70° relative to the target normal. To avoid air breakdown and nonlinear effects in air for high fluence irradiation, the target is placed 0.5 mm forward from the focal position. The laser pulses have a Gaussian spatial profile, with an average spot size of 40 μm at 1/e intensity, measured at the target surface position at normal incidence. The effective spot size at oblique incidences is evaluated by dividing the spot size by $\cos\theta$. Laser fluence is determined by the effective spot size and the energy of the incident laser pulse. The laser fluence is controlled from 0.05 to 2.5 J/cm^2 by using a polarizer together with a half-wave plate to change the laser energy. Laser pulses are split by a quartz plate, and reflected pulses are guided to a photodiode to monitor the energy stability of pulses. The standard deviation of energy stability is kept within ±2.5% in this experiment. The polarization extinction ratio is greater than 200. The depths of ablation craters are measured with a confocal laser scanning microscope (HL-150, Lasertec). The number of irradiated pulses is controlled for each fluence to make a crater deep enough to be measurable; this requires between 50 and 230 000 pulses. At normal incidence, the crater is deepest at its center. However, the position of the deepest point shifts in the laser propagation direction at oblique incidences. Here, the ablation rate is defined by the depth at the deepest position divided by the number of irradiated pulses.

Figure 1 shows the ablation rates for different laser incidence angles with *p*-polarization (Fig. 1(a)) and *s*-polarization (Fig. 1(b)). The ablation rate at normal incidence is shown in both panels for comparison. For *p*-polarization, the ablation rates do not depend on the laser incidence angle when the fluence is greater than 1 J/cm^2. However, as the laser fluence decreases, the ablation rates become slightly larger at oblique incidence angles than at normal incidence. By contrast, the ablation rates for *s*-polarization show a qualitatively different relation with laser fluence. The ablation rates decrease rapidly as the incidence angle is increased in all fluence ranges, and particularly with a fluence of less than 1 J/cm^2. For large incidence angles, the ablation rate decreases markedly as the angle is increased when the fluence is less than 0.7 J/cm^2. Compared with the ablation rate at normal incidence, the ablation rate due to an *s*-polarized laser at 70° incidence is two orders of magnitude lower for fluences less than 0.7 J/cm^2.

Figure 2 shows the ablation rate dependence on laser fluence for normal incidence and for oblique incidence, respectively. The solid lines and dashed lines show the least-squares fitting by Eq. (1) and Eq. (2) in the high and middle fluence ranges, respectively. The ablation rate dependences for oblique incidence as well as the ablation rate dependence for normal incidence are well fitted by logarithmic expressions. The fitted parameter values for normal incidence, namely, $F_{\mathrm{th,h}} = 0.39$ J/cm^2, $F_{\mathrm{th,m}} = 0.16$ J/cm^2, $l = 58$ nm, and $d = 6.7$ nm, are similar to those in other reports.[8,14] The values obtained for oblique incidence are listed in Table I. The small variation in slopes of the solid lines in Fig. 2 means that the differences in values of l are small. The small differences are reasonable given that ablation in the high fluence range is determined by the thermal diffusion of hot

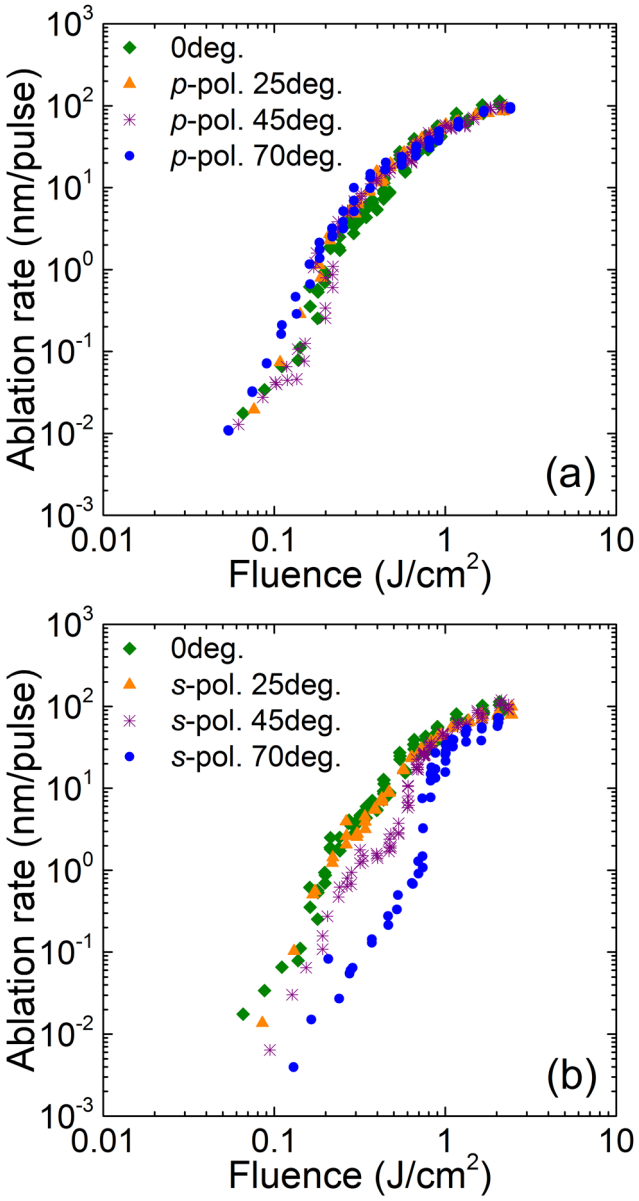

FIG. 1. Ablation rate dependence on laser fluence for (a) *p*-polarization and (b) *s*-polarization. The common ablation rate at normal incidence is shown in both panels.

electrons, as is also the case for normal incidence. Thermal diffusion takes a much longer time than a single pulse. Under the assumption that the laser pulse is merely an energy source, the behavior of hot electrons is independent of the laser incidence angle and polarization. In contrast, the slopes of the dashed lines are quite different from each other. The values of d vary widely, and dependence on incidence angle differs between *s*- and *p*-polarizations. As the incidence angle is increased, the value of d for *p*-polarization (d_p) and *s*-polarization (d_s) changes from 6.7 to 21 nm and from 6.7 to 0.47 nm, respectively. When light travels into metal from air, the theoretical optical penetration depth as a function of incidence angle is given by the following equation:

$$\left[2\mathrm{Im}\left(\frac{\omega}{c}\sqrt{(n+i\kappa)^2-\sin^2\theta}\right)\right]^{-1}, \qquad (3)$$

where ω is the angular frequency of light, c is the speed of light through vacuum, and n and κ are the refractive index

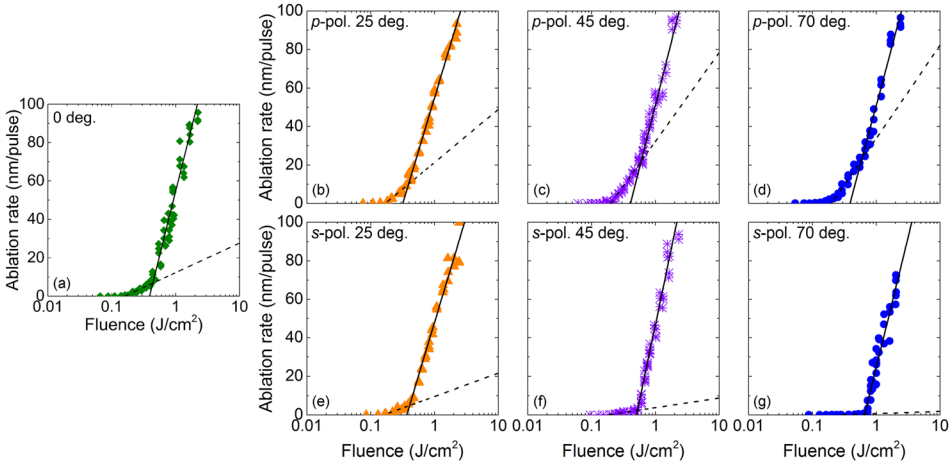

FIG. 2. Ablation rates for (a) normal incidence, for *p*-polarization at (b) 25°, (c) 45°, and (d) 70° incidence, and for *s*-polarization at (e) 25°, (f) 45°, and (g) 70° incidence. Solid and dashed lines were fit by the least-squares method to Eqs. (1) and (2), respectively. Fitting parameter values are listed in Table I.

and extinction coefficient of the metal, respectively. The function Im gives the imaginary part of a complex number. It is noteworthy that the optical penetration depth is independent of laser polarization, and the reduction of laser intensity depends only on the depth from the surface, even if the transmitted light propagates obliquely. The optical penetration depth given by Eq. (3) is 12.5–12.3 nm for incidence angles 0°–90° with a wavelength of 805 nm ($n = 0.25$, $\kappa = 5.1$).[35] Although the optical penetration depth depends only minimally on the incidence angle, the slopes of the dashed lines in Fig. 2 are different from each other. Two explanations are considered to account for the disagreement between the optical penetration depth and the value of d. One is that unknown effects alter the optical penetration depth according to incidence angle. Equation (3) is derived from the boundary condition between different mediums for a general electromagnetic wave. Here, the effect of the high intensity and short pulse duration of the femtosecond laser have not been taken into account. An alternative explanation is that the optical penetration depth is unrelated to ablation rate at middle fluences. Instead, the key value for determining the scale of the ablation rate at a middle fluence might be another length parameter. The dependence of ablation rate on incidence angle and polarization as obtained in this experiment suggests the existence of some undiscovered factor for ablation in the middle fluence range. Hereinafter, d will be regarded as an effective penetration depth because it is unlikely that d corresponds to the optical penetration depth. The relations between effective penetration depth d and the incidence angle for *p*- and *s*-polarizations are plotted in Fig. 3. Though the electric field at normal incidence and at oblique incidences with *s*-polarization consists of only the component parallel to the surface, the electric field for oblique incidence angles with *p*-polarization includes components orthogonal to the surface. Under the assumption that an electric field orthogonal to the substrate contributes to ablation, the change in d_p might be proportional to $\sin\theta$. The dashed curve in Fig. 3 is obtained by fitting $d_0 + A\sin^N\theta$ by the least-squares method, which yields the values $A = 16$ and $N = 1.1$. Here, $d_0 = 6.7$ nm is the effective penetration depth at normal incidence. Therefore, the effective penetration depth for *p*-polarization can be approximated as

$$d_p = d_0 + A\sin\theta. \tag{4}$$

For *s*-polarization, the electric field is parallel to the target surface, and the effective penetration depth decreases as the incidence angle is increased. Simple drilling in the direction of laser propagation will result in a depth-to-length ratio proportional to $\cos\theta$. The solid curve shown in Fig. 3 is obtained by fitting $d_0\cos^M\theta$ to the effective penetration

TABLE I. Parameter values for ablation rates obtained by least-squares fitting.

Polarization and incidence angle	l (nm)	$F_{th,\,h}$ (J/cm^2)	R_h	d (nm)	$F_{th,\,m}$ (J/cm^2)	R_m
0°	58	0.39	0.37	6.7	0.16	0.82
s-polarization 25°	48	0.37	0.45	5.2	0.16	0.86
s-polarization 45°	69	0.51	0.43	2.2	0.18	0.95
s-polarization 70°	59	0.66	0.62	0.47	0.25	0.99
p-polarization 25°	48	0.32	0.37	12	0.17	0.70
p-polarization 45°	57	0.41	0.41	20	0.20	0.58
p-polarization 70°	54	0.39	0.42	21	0.20	0.56

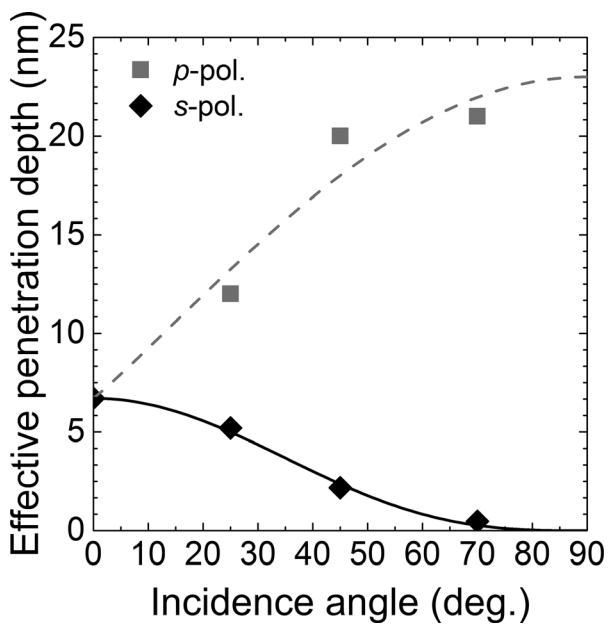

FIG. 3. Relation between effective penetration depth d and incidence angle for *p*-polarization (gray squares) and *s*-polarization (black diamonds). Solid and dashed curves show $d_0\cos^{3.0}\theta$ and $d_0 + 16\sin^{1.1}\theta$, respectively.

depth of *s*-polarization by the least-squares method, which gives $M = 3.0$. From this, the effective penetration depth of copper for oblique incidence with *s*-polarization can be approximated as

$$d_s = d_0 \cos^3\theta. \quad (5)$$

This shows that ablation by *s*-polarized laser pulses are strongly suppressed as the incidence angle increases.

In Eqs. (1) and (2), the values of reflectance determine only the ablation threshold fluence. Though it is ambiguous that the parameter d is related to optical penetration depth, the independence of reflectance and penetration depth is reasonable since the penetration is assessed after transmission. The evaporation threshold energy per volume E_{th} is 42.2 kJ/cm^3 for copper.[13] The values of R_h and R_m are listed in Table I. The reflectance is strongly influenced by surface morphology.[36,37] The craters produced by ablation are covered in many nano- and micro-structures because multi-pulse irradiation is used to create a crater deep enough to be measureable. The difference between R_h and R_m suggests that the surface morphology created by high fluence irradiation absorbs more than that created by middle fluence irradiation, as has been reported previously.[36] Figure 4 shows the dependences of reflectance on incidence angle for ideal copper, as calculated by the Fresnel equations for *p*- (dashed curve) and s-polarizations (solid curve), and the values of R_m for *p*- (gray squares) and *s*-polarizations (black diamonds). The dependences of R_m on incidence angle show qualitatively the same trends as the Fresnel equations, but the absolute values are different. This suggests that the reflectance follows the Fresnel equations in the middle fluence range, and that the surface morphology created by middle fluence irradiation modulates reflectance.

The dependence of ablation rate on incidence angle and polarization mode was investigated for copper. The ablation rate at oblique incidence angles showed a logarithmic relation, as did the ablation rate at normal incidence. In the high fluence range, the observed dependence of the ablation rate can be explained by the hot electron diffusion length for all irradiation conditions. However, the ablation rate in the middle fluence range exhibited a different dependence from that predicted theoretically using optical penetration depth, as shown in the difference in the slopes of dashed lines in Fig. 2. As the incidence angle was increased, the ablation rate increased slightly for *p*-polarization but decreased rapidly for *s*-polarization. The dependence of reflectance on the incidence angle as estimated from a logarithmic expression for the middle fluence range agrees qualitatively with that obtained from the Fresnel equations. In the middle fluence range, the dependence of ablation rate on laser fluence for irradiation at oblique incidence angles (including at normal incidence) for *p*- and *s*-polarizations were found to be

$$L_p = (d_0 + A\sin\theta)\ln(F/F_{th,m}),$$
$$L_s = d_0\cos^3\theta\ln(F/F_{th,m}),$$

respectively. These simple formulas for copper should be useful for future studies of laser processing and optics damage.

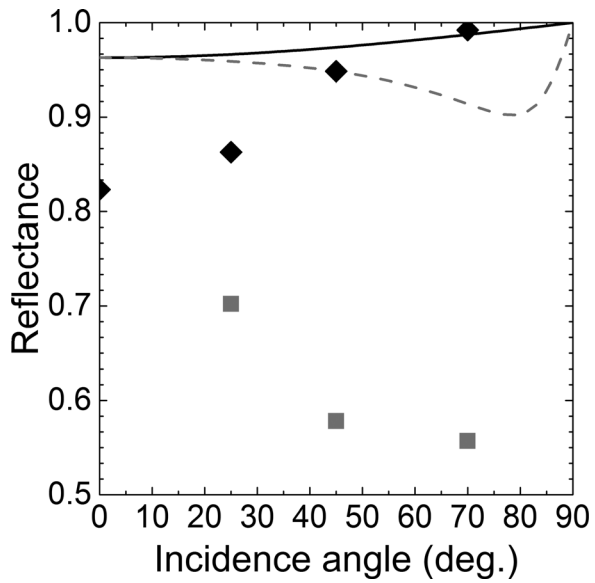

FIG. 4. Reflectance as a function of incidence angle according to the Fresnel equations for *p*-polarization (dashed curve) and *s*-polarization (solid curve). Gray squares and black diamonds indicate reflectance in the middle fluence range for *p*- and *s*-polarizations, respectively.

We thank T. Kanaya and K. Nishida for their assistance with confocal laser scanning microscopy. This research was financially supported by JSPS KAKENHI Grant Nos. 25·4829 and 25420728, and by the Amada Foundation (AF-2011215); it was also partially supported by a Grant-in-Aid for the Global COE program (Next Generation of Physics, Spun from Universality and Emergence) from MEXT.

[1]M. Hashida, H. Mishima, S. Tokita, and S. Sakabe, Opt. Express **17**, 13116 (2009).
[2]B. N. Chichkov, C. Momma, S. Nolte, F. von Alvenseben, and A. Tünnermann, Appl. Phys. A **63**, 109 (1996).
[3]K. Okamuro, M. Hashida, Y. Miyasaka, Y. Ikuta, S. Tokita, and S. Sakabe, Phys. Rev. B **82**, 165417 (2010).
[4]A. Y. Vorobyev, V. S. Makin, and C. Guo, J. Appl. Phys. **101**, 034903 (2007).
[5]M. Barberoglou, V. Zorba, A. Pagozdis, C. Fotakis, and E. Stratakis, Langmuir **26**, 13007 (2010).
[6]M. Hashida, Y. Miyasaka, Y. Ikuta, S. Tokita, and S. Sakabe, Phys. Rev. B **83**, 235413 (2011).
[7]S. Matsumoto, A. Yane, S. Nakashima, M. Hashida, M. Fujita, Y. Goto, and S. Takahashi, J. Am. Chem. Soc. **129**, 3840 (2007).
[8]M. Hashida, A. F. Semerok, O. Gobert, G. Petite, Y. Izawa, and J.-F. Wagner, Appl. Surf. Sci. **197–198**, 862 (2002).
[9]S. E. Kirkwood, M. T. Taschuk, Y. Y. Tsui, and R. Fedosejevs, J. Phys. Conf. Ser. **59**, 591 (2007).
[10]M. Hashida, Y. Ikuta, Y. Miyasaka, S. Tokita, and S. Sakabe, Appl. Phys. Lett. **102**, 174106 (2013).
[11]M. Shimizu, M. Hashida, Y. Miyasaka, S. Tokita, and S. Sakabe, Appl. Phys. Lett. **103**, 174106 (2013).
[12]M. Hashida, A. Semerok, O. Gobert, and G. Petite, Proc. SPIE **4423**, 178 (2001).
[13]B. H. Christensen, K. Vestentoft, and P. Balling, Appl. Surf. Sci. **253**, 6347 (2007).
[14]S. Nolte, C. Momma, H. Jacobs, A. Tünnermann, B. N. Chichkov, B. Wellegehausen, and H. Welling, J. Opt. Soc. Am. B **14**, 2716 (1997).
[15]S. Preuss, A. Demchuk, and M. Stuke, Appl. Phys. A **61**, 33 (1995).
[16]P. T. Mannion, J. Magee, E. Coyne, G. M. O'Connor, and T. J. Glynn, Appl. Surf. Sci. **233**, 275 (2004).
[17]R. Le Harzic, D. Breitling, M. Weikert, S. Sommer, C. Föhl, F. Dausinger, S. Valette, C. Donnet, and E. Audouard, Appl. Phys. A **80**, 1589 (2005).
[18]A. E. Wynne and B. C. Stuart, Appl. Phys. A **76**, 373 (2003).

[19]J. P. Colombier, P. Combis, F. Bonneau, R. Le Harzic, and E. Audouard, Phys. Rev. B **71**, 165406 (2005).
[20]M. E. Povarnitsyn, T. E. Itina, M. Sentis, K. V. Khishchnko, and P. R. Levashov, Phys. Rev. B **75**, 235414 (2007).
[21]B. Wu and Y. C. Shin, Appl. Surf. Sci. **253**, 4079 (2007).
[22]W. Hu, T. C. Shin, and G. King, J. Phys. D **45**, 355204 (2012).
[23]C. Schäfer and H. M. Urbassek, Phys. Rev. B **66**, 115404 (2002).
[24]S. Y. Wang, Y. Ren, C. W. Cheng, J. K. Chen, and D. Y. Tzou, Appl. Surf. Sci. **265**, 302 (2013).
[25]S. I. Anisimov, B. L. Kapeliovich, and T. L. Perel'man, JETP **39**, 375 (1974).
[26]C. Hnatovsky, V. G. Shvedov, and W. Krolikowski, Opt. Express **21**, 12651 (2013).
[27]S. Nolte, C. Momma, G. Kamlage, A. Ostendorf, C. Fallnich, F. von Alvensleben, and H. Welling, Appl. Phys. A **68**, 563 (1999).
[28]R. Torres, T. Kaempfe, M. Delaigue, O. Parriaux, C. Honninger, J. Lopez, R. Kling, and E. Mottay, J. Laser Micro. Nanoeng. **8**, 188 (2013).
[29]Q. Z. Zhao, S. Malzer, and L. J. Wang, Opt. Lett. **32**, 1932 (2007).
[30]J. Wang and C. Guo, J. Appl. Phys. **100**, 023511 (2006).
[31]T. Y. Yong and C. Guo, J. Appl. Phys. **108**, 073523 (2010).
[32]M. Hashida, S. Namba, K. Okamuro, S. Tokita, and S. Sakabe, Phys. Rev. B **81**, 115442 (2010).
[33]Y. Miyasaka, M. Hashida, Y. Ikuta, K. Otani, S. Tokita, and S. Sakabe, Phys. Rev. B **86**, 075431 (2012).
[34]S. Amoruso, X. Wang, C. Altucci, C. de Lisio, M. Armenante, R. Bruzzese, and R. Velotta, Appl. Phys. Lett. **77**, 3728 (2000).
[35]P. B. Johnson and R. W. Christy, Phys. Rev. B **6**, 4370 (1972).
[36]A. Y. Vorobyev and C. Guo, J. Appl. Phys. **110**, 043102 (2011).
[37]B. Hopp, T. Smausz, T. Csizmadia, C. Vass, C. Tapái, B. Kiss, M. Ehrhardt, P. Lorenz, and K. Zimmer, Appl. Phys. A **113**, 291 (2013).